Electronic band structure and low-temperature transport properties of the type-I clathrate Ba8NixGe46-x-y y

Umut Aydemir, Christophe Candolfi, Alim Ormeci, Michael Baitinger, Ulrich Burkhardt, Niels Oeschler, Franck Steglich, Yuri Grin

Electronic band structure and low-temperature transport properties of the type-I clathrate $Ba_8Ni_xGe_{46-x-y}\square_y$

U. Aydemir[1,2,†], C. Candolfi[1,‡], A. Ormeci[1,*], M. Baitinger[1], U. Burkhardt[1], N. Oeschler[1], F. Steglich[1], Yu. Grin[1,*]

[1] *Max-Planck-Institut für Chemische Physik fester Stoffe, 01187 Dresden, Germany*

[2] *Koç University, Rumelifeneri Yolu, Sarıyer, 34450 Istanbul, Turkey*

[*] Corresponding authors: ormeci@cpfs.mpg.de, grin@cpfs.mpg.de

[†] Present address: Department of Applied Physics and Materials Science, California Institute of Technology, 1200 E California Blvd, Pasadena, CA 91125, USA

[‡] Present address: Institut Jean Lamour, UMR 7198 CNRS – Université de Lorraine, Parc de Saurupt, CS 50840, 54011 Nancy, France

Abstract

We present the evolution of the low-temperature thermodynamic, galvanomagnetic and thermoelectric properties of the type-I clathrate $Ba_8Ni_xGe_{46-x-y}\square_y$ with the Ni concentration studied on polycrystalline samples with $0.0 \leq x \leq 6.0$ by means of specific heat, Hall effect, electrical resistivity, thermopower and thermal conductivity measurements in the 2 – 350 K temperature range and supported by first-principles calculations. The experimental results evidence a $2a\times2a\times2a$ supercell described in the space group $Ia\bar{3}d$ for $x \leq 1.0$ and a primitive unit cell $a\times a\times a$ (space group $Pm\bar{3}n$) above this Ni content. This concentration also marks the limit between a regime where both electrons and holes contribute to the electrical conduction ($x \leq 1.0$) and a conventional, single-carrier regime ($x > 1.0$). This evolution is traced by the

variations in the thermopower and Hall effect with *x*. In agreement with band structure calculations, increasing the Ni content drives the system from a nearly-compensated semimetallic state (x = 0.0) towards a narrow-band-gap semiconducting state (x = 4.0). A crossover from an *n*-type to a *p*-type conduction occurs when crossing the x = 4.0 concentration *i.e.* for x = 4.1. The solid solution $Ba_8Ni_xGe_{46-x-y}\square_y$ therefore provides an excellent experimental platform to probe the evolution of the peculiar properties of the parent type-I clathrate $Ba_8Ge_{43}\square_3$ upon Ge/Ni substitution and filling up of the vacancies, which might be universal among the ternary systems at low substitution levels.

I. Introduction

Type-I clathrates represent a class of prospective thermoelectric materials for high-temperature power generation applications.[1-4] Low thermal conductivity is an inherent property of these compounds and arises from their cage-containing crystal structure (Figure 1).[4,5] This characteristic is one of the requisites which need to be satisfied in a thermoelectric material whose efficiency is described by the dimensionless figure of merit $ZT = \alpha^2 T / \rho\kappa = PT / \kappa$ where α is the thermopower, ρ is the electrical resistivity, κ is the total thermal conductivity, T is the absolute temperature and $P = \alpha^2 / \rho$ is the power factor.[6] The large number of elements which can substitute the framework atoms enables a fine tuning of the carrier concentration to optimize the *ZT*.[2] In this regard, the Zintl-Klemm concept plays a central role in predicting whether a clathrate is a metal or a semiconductor.[7]

Recent investigation has proved substitutions of framework elements to be an efficient way to enhance the thermoelectric properties of Ge-based type-I clathrates.[8,9] The presence of several elements in the framework leads to reduced lattice thermal conductivity together with optimized power factors arising from the proximity to a semiconducting state. In particular, a

maximum *ZT* of 1.2 was achieved at 1000 K in the $Ba_8Ni_{0.31}Zn_{0.52}Ga_{13.06}Ge_{32.2}$ clathrate.[10] The knowledge about the influence of substitutions on transport behavior may therefore help to further optimize the thermoelectric properties of clathrates. While this issue has been settled for several elements such as Cu, Zn or Ga, some other elements (such as Al, In or Ni) still lack a detailed investigation both from theoretical and experimental points of view.[2]

Prior investigations on clathrates in the Ba-Ni-Ge system have shown that a metal-insulator and an *n*-type to *p*-type transitions set in, the latter feature being rarely achieved in type-I clathrates.[11,12] Despite the fact that the composition at which this crossover occurs remained debated until recently,[11,13] it was clearly established that switching the electrical conduction from *n*-type to *p*-type strongly influences the thermal transport which shows a glass-like behavior in the *p*-type samples.[11] A final conclusion regarding this issue has been drawn from high-temperature transport measurements on $Ba_8Ni_xGe_{46-x-y}\square_y$ specimens with compositions $0.2 \leq x \leq 6.0$ demonstrating that the crossover sets in between $x = 4.0$ and 4.1.[14] These investigations further revealed that the maximum Ni content at 700 °C is $x \approx 4.2$ atoms per unit cell. This limit, significantly lower than those previously suggested, is consistent with the study of Shi *et al.*[10] showing by *ab initio* calculations that the composition $x = 6.0$ is energetically unstable. These theoretical findings were experimentally confirmed by x-ray diffraction data and transport property measurements revealing a limit of $x \approx 4.0$ (Ref.10) and were coherent with the growth of large *n*-type single crystals with a composition $Ba_8Ni_{3.5}Ge_{42.1}\square_{0.4}$.[15]

The possibility to drive the system close to a semiconducting state together with an *n*- to *p*-type crossover in the electrical conduction may provide an interesting experimental platform to design thermoelectric materials of *p*- and *n*-type on the same elemental basis. Further, the opportunity to extend the Ni concentration range down to $x = 0$ may also shed light on the nearly-compensated semimetallic state of $Ba_8Ge_{43}\square_3$ and on its evolution upon

filling up of the vacancies.[16]

Herein, to address these as yet unexplored issues, we report a joint theoretical and experimental study of the electronic band structure and low-temperature transport properties of the $Ba_8Ni_xGe_{46-x-y}\square_y$ clathrate phase in the actual compositional range $0.0 \leq x \leq 4.1$. Our results show a smooth evolution of the transport properties from a nearly-compensated semimetallic state for $Ba_8Ge_{43}\square_3$ towards a semiconducting behavior as the Ni content approaches $x = 4.0$. A crossover from *n*-type to *p*-type conduction occurring above this concentration is confirmed in agreement with first-principles calculations.

II. Experimental and computational details

Polycrystalline samples were synthesized by direct reaction of the elements followed by either annealing or steel-quenching. All the details concerning the preparation are described in detail in Ref. 14, 17 and 18. The crystal structure, phase purity and homogeneity range of the samples were investigated by powder x-ray diffraction (PXRD), scanning electron microscopy (SEM) and wavelength dispersive x-ray spectroscopy (WDXS).[14] X-ray absorption spectra of the clathrate samples in the system Ba – Ni – Ge have been determined close to the Ni *K*-edge (8333 eV) in transmission mode at EXAFS beamline C of HASYLAB at German Electron Synchrotron (DESY).

Transport property measurements were performed on bar-shaped samples cut from the steel-quenched samples into typical dimensions of $2\times2\times6$ mm^3 with a diamond-wire saw. Electrical resistivity, thermopower and thermal conductivity were simultaneously measured using the thermal transport option of a physical property measurement system (PPMS-Quantum Design) in the temperature range 5 – 350 K. Hall effect measurements were carried out with an ac transport option of a PPMS between 2 and 300 K under magnetic fields ranging

from -5 to 5 T. A five-point method using copper wires attached onto the sample with a tiny amount of silver paste was used. To dismiss any magnetoresistive contribution which may obscure the intrinsic Hall signal, the antisymmetric part of the transverse electrical resistivity, ρ_{xy}, under magnetic field reversal following the formula $(\rho_{xy}(+\mu_0 H) - \rho_{xy}(-\mu_0 H))/2$ was determined. Specific heat measurements under zero magnetic field were performed with a PPMS by a standard relaxation method between 1.9 and 15 K and up to 300 K for selected samples.

Electronic structure calculations were carried out using the all-electron, full-potential local orbital (FPLO) method.[20] Perdew-Wang parameterization for the local density approximation (LDA) to the density functional theory was employed to account for the exchange-correlation effects.[21] The clathrate $Ba_8Ni_xGe_{46-x-y}\square_y$ contains framework vacancies for all x less than 4.0, in such a way that the 6*c* Wyckoff position in the space group $Pm\bar{3}n$ (no. 223) of the type-I clathrate structure may be occupied by Ge, Ni or be vacant. The treatment of this disorder requires using supercells in the first-principles calculations. Supercells were determined through the group-subgroup relations by paying attention to the way the 6*c* position is split in possible subgroups. A convenient starting point for most of the compositions is the space group $Ia\bar{3}d$ (no. 230) with cubic lattice parameter 2*a*. Apart from the compositions with $x = 2.0$, $y = 2.0$ and $x = 4.0$, $y = 0.0$ (for which space group $P4_122$ (no. 91) based on the $a \times a \times 2a$ supercell was used), all other cases were calculated in either $Ia\bar{3}d$ or one of its subgroups (four formula units in the primitive cell in all cases, because all subgroups considered are body-centric). The x values used are 0.5, 1.0, 1.5, 2.0, 3.0, 4.0 and 4.5 combined with suitable y values (Table I). The values of the lattice parameters and atomic positions were taken from the experimental data on cubic crystal structure obtained for compositions close to the ones used in the calculations.

III. Results and discussion

A. Chemical and structural characterizations

Polycrystalline samples of $Ba_8Ni_xGe_{46-x-y}\square_y$ were synthesized by two routes: by steel-quenching ($0.2 \leq x \leq 3.5$, Ref. 18) and by steel-quenching followed by an annealing step at 973 K for 4 days ($3.5 < x \leq 6.0$). The nominal and actual compositions of the different samples investigated together with the lattice parameters are listed in Table II. Hereafter, we shall always use the actual composition to label the samples. Samples with low Ni contents ($0.2 \leq x \leq 1.0$; $2.0 \leq y \leq 3.0$), contain clathrate-I phase in the superstructure described in the space group $Ia\bar{3}d$ (no. 230) together with small amounts of α-Ge or Ba_6Ge_{25} (Table II). Samples with compositions $1.5 \leq x \leq 3.5$ consist of clathrate-I phase in the space group $Pm\bar{3}n$ (no. 223) along with, for some compositions, small inclusions of α-Ge and/or Ba_6Ge_{25}. Samples prepared with $x > 4.2$ showed increasing amounts of NiGe and/or $BaGe_2$ as secondary phases suggesting that $x \approx 4.2$ is the highest limit of the homogeneity range, contrary to other reported studies.[11,12,22,23] Note that because the $Ba_8Ni_6Ge_{40}$ sample with an actual Ni content of $x = 4.2$ contains large amount of by-products, we limited our transport properties investigation to the compositional range $0.2 \leq x \leq 4.1$.

The clathrate phase with low Ni content can be considered as a solid solution of Ni in the binary $Ba_8Ge_{43}\square_3$ for $0.2 \leq x \leq 1.0$ (a = 21.3079(2) Å - 21.3189(1) Å, Figure 2). In this range, the vacancies can be filled up by Ni atoms ($Ba_8Ge_{43}Ni_x\square_{3-x}$), Ni atoms can substitute Ge atoms with the number of vacancies kept constant ($Ba_8Ni_xGe_{43-x}\square_3$) or both mechanisms can take place simultaneously ($Ba_8Ni_xGe_{43-y}\square_z$; $z = 3 - x + y$). The lattice parameter of the clathrate phase increases with the Ni content. A second existence field can be further divided into two ranges. In the first range ($1.0 < x \leq 3.5$), Ni atoms progressively fill the vacancies (a

= 10.6612(1) Å - 10.6803(1) Å). The lattice parameter increases further with x up to a maximum achieved at x = 3.5 (a = 10.6803(1) Å, see Table II). The value of the lattice parameter is in good agreement with that established for single crystalline $Ba_8Ni_{3.5}Ge_{42.1}\square_{0.4}$ (a = 10.6798(2) Å),[15] but significantly larger than those previously reported for samples supposedly prepared with higher Ni contents ($x \geq 5$, see Table II).[11,22,23] In the second range ($3.5 < x \leq 4.2$), the lattice parameter slightly decreases down to a = 10.6771(1) Å for x = 4.1 and remains almost constant until x = 4.2 sample (10.6765(1) Å) pointing to the Ge-by-Ni substitution as the only mechanism in this Ni-content range (Figure 2).

The compositions of the samples were determined by WDXS (Table II). The Ba content was considered to be 8 atoms per formula unit as determined from the single-crystal structure analysis. From the WDXS results, the lower and upper limits of the homogeneity range in the present series of samples were determined to be 0.2 and 4.2 Ni atoms per formula unit.

It was shown previously for several families of oxide compounds *e.g.*, $KNiIO_6$, $LiNiO_2$, NiO, $LaNiO_3$, $LaNi_2O_5$ or $LaNiO_2$ that the x-ray absorption edge energy shifts to higher values by increasing valence of the Ni atoms.[24,25] In this study, besides clathrate samples (Figure 3a), the spectra of Ni foil, NiGe, NiI_2 and NiO were also recorded for comparison (Figure 3b). As shown in Figure 3a, the Ni *K*-edge XANES region of the clathrate samples shows almost identical features. Figure 3b shows that the position of the Ni absorption edge of the clathrate samples is very close to those of Ni foil and NiGe, but is very well separated from those of NiO and NiI_2. Hence, we can conclude that the electronic state of Ni in the Ba-Ni-Ge system is close to that in elemental Ni.

B. Electronic structure

Performing electronic structure calculations for $Ba_8Ni_xGe_{46-x-y}\square_y$ requires modeling of both the composition of the particular clathrate and the disorder stemming from the partial occupancy of the 6*c* Wyckoff position. Moreover, different vacancy concentrations for the same Ni content have to be considered. Vacant sites can be taken into account by using supercells (Table I). Structure models with different 6*c* site occupancies were chosen for the compositions $Ba_8Ni_xGe_{43-x}\square_3$ and $Ba_8Ni_xGe_{43}\square_{3-x}$ for x = 0.5 and 1.0, while for x = 2.0 and 3.0 the models $Ba_8Ni_xGe_{43}\square_{3-x}$ and $Ba_8Ni_xGe_{42}\square_{4-x}$ are employed. The Ni content x = 1.5 is considered as a special case, therefore all models mentioned above are applied to this case, namely, $Ba_8Ni_{1.5}Ge_{41.5}\square_3$, $Ba_8Ni_{1.5}Ge_{43}\square_{1.5}$, and $Ba_8Ni_{1.5}Ge_{42}\square_{2.5}$. For x = 4.0 and 4.5, no vacancies at the 6*c* position are assumed.

Comparison of electronic total energies may be helpful in determining which model is preferred for a specific Ni content. This may also provide a general idea about the dependence of the vacancy concentration on the Ni content. The balances considered are as follows:

$$Ba_8Ni_xGe_{43-x}\square_3 + x\alpha\text{-Ge} \rightarrow Ba_8Ni_xGe_{43}\square_{3-x} + \Delta E_1(x) \quad (1)$$

$$Ba_8Ni_xGe_{42}\square_{4-x} + \alpha\text{-Ge} \rightarrow Ba_8Ni_xGe_{43}\square_{3-x} + \Delta E_2(x) \quad (2)$$

A positive value for $\Delta E_i(x)$ means the clathrate $Ba_8Ni_xGe_{43}\square_{3-x}$ on the right-hand-side is preferred implying that the binary clathrate $Ba_8Ge_{43}\square_3$ acts as a parent compound for that Ni content. The details pertaining to these calculations will be presented elsewhere. The main findings may be summarized in the following way: $\Delta E_1(x)$ is positive for x = 0.5, 1.0 and 1.5, whereas $\Delta E_2(x)$ is negative for x = 2.0 and 3.0. Hence, for x between 0.5 and 1.5, Ni fills up the vacancies of $Ba_8Ge_{43}\square_3$, but for x = 2.0 and 3.0, Ni fills up the vacancies of the

hypothetical compound $Ba_8Ge_{42}\square_4$ (with four vacancies at 6*c* sites). Note that the balances (1) and (2) can be used only to determine which of the compositions considered is preferred; the question of site preference by Ni atoms is a highly demanding task and is out of the scope of this paper.

In light of the above results the electronic structure of $Ba_8Ni_xGe_{46-x-y}\square_y$ can be examined in two separate categories: (i) compositions $Ba_8Ni_xGe_{43}\square_{3-x}$ with constant Ge content of 43 atoms per unit cell, for which voids are replaced by Ni atoms (x = 0.0, 0.5, 1.0, 1.5); (ii) compositions $Ba_8Ni_xGe_{42}\square_{4-x}$ with Ge content of 42 atoms per unit cell (x = 2.0, 3.0 and 4.0). The densities of states (DOS) for low Ni content ($x \leq 1.5$) are shown in Figure 4. We observe that, taking the electronic structure of $Ba_8Ge_{43}\square_3$ (Figure 4a) as reference,[16] the inclusion of Ni into the clathrate-I structure has no significant effect on the DOS. The gap at about 0.5 eV below the Fermi energy (E_F) is preserved at all Ni concentrations ($x \leq 1.5$). In an empty ckathrate-I Ge_{46}, the Ge atoms are each fourfold coordinated so that this empty clathrate should have a band gap. Our own calculations on the fully-optimized Ge_{46} structure give a gap of 1.22 eV (in very good agreement with that obtained by Zhao *et al*.[26]), which survives in the binary compound $Ba_8Ge_{43}\square_3$ though with a reduced width of about 0.2 eV. The 16 extra electrons due to Ba atoms are compensated only partially by the absence of three Ge atoms at the 6*c* sites leading to the following electron balance: $[Ba^{2+}]_8[(3b)Ge^-]_{12}\ [(4b)Ge^0]_{31} \cdot 4e^-$ where (3b) and (4b) denote the three-bonded and four-bonded Ge atoms, respectively. Thus, the net number of extra electrons in $Ba_8Ge_{43}\square_3$ is four per formula unit, and consequently the number of electrons between the top of this gap and E_F is 16 for the primitive cell, which contains four formula units.[18] This electron count also remains unchanged upon Ni substitution. Therefore, the additional states stemming from Ni electrons do not introduce new features near E_F. The only clearly discernible change in the DOS due to Ni atoms is the appearance of some states between -5 and -4.5 eV.

The electronic DOS for $Ba_8Ni_xGe_{42}\square_{4-x}$ with x = 1.0, 2.0, 3.0 and 4.0 are presented in Figure 5. The x = 1.0 case is provided for allowing a comparison with the DOS of $Ba_8NiGe_{43}\square_2$. We note that although the Ni content is changing the general features of the DOS stay essentially the same. A prominent feature is that the Fermi energy is at a pseudo-gap in all cases. This gap is expected in the hypothetical clathrate $Ba_8Ge_{42}\square_4$, where the 16 electrons from the Ba atoms will be compensated by the absence of four Ge atoms at the 6*c* site yielding $[Ba^{2+}]_8[(3b)Ge^{-}]_{16}[(4b)Ge^0]_{26}$ with no excess charge. When Figures 4 and 5 are considered together, we infer that Ni atoms in these clathrate compounds should exhibit an oxidation state of 0. The electron balances can thus be written as follows:

$$Ba_8Ni_xGe_{43}\square_{3-x}\text{: } [Ba^{2+}]_8[(4b)Ni^0]_x[(3b)Ge^{-}]_{12}[(4b)Ge^0]_{31} \cdot 4e^{-}$$

$$Ba_8Ni_xGe_{42}\square_{4-x}\text{: } [Ba^{2+}]_8[(4b)Ni^0]_x[(3b)Ge^{-}]_{16}[(4b)Ge^0]_{26}$$

X-ray absorption spectra measurements (see Figure 3) carried out on $Ba_8Ni_xGe_{46-x-y}\square_y$ experimentally confirm that Ni atoms in the clathrate behave similarly to the Ni atoms in the elemental solid. Figures 4 and 5 also show that in the system $Ba_8Ni_xGe_{46-x-y}\square_y$, two basic types of electronic structure are present corresponding to $Ba_8Ni_xGe_{43}\square_{3-x}$ and to $Ba_8Ni_xGe_{42}\square_{4-x}$ for $x \leq 4.0$. The absence of a real band gap in the series $Ba_8Ni_xGe_{42}\square_{4-x}$, especially for the x = 4.0 case, deserves further comments. Various test calculations suggest that how deep the pseudo-gap is or, in other words, how close the pseudo-gap to a real gap is depends sensitively on the Ni-Ge3 and Ge1-Ge3 distances used in the calculations. Optimization of the atomic coordinates in primitive cells containing ~100 or 200 atoms by an all-electron method is very time consuming, and therefore was not attempted herein. This point should be kept in mind when comparing the experimental findings to the theoretical ones.

When the Ni content is increased above x = 4.0, the Fermi energy falls below the

gap/pseudo-gap. Figure 6 shows that a transition occurs from *n*-type DOS (E_F above gap) to *p*-type DOS (E_F below the gap) through the E_F at the pseudo-gap case. DOS for x = 4.5 and 6.0 were calculated with all Ni atoms placed at the 6*c* site. The values of DOS at the Fermi energy, $N(E_F)$, for these cases are considerably large: 308.9 and 316.6 states Ry^{-1} per formula unit, respectively. In contrast, the highest $N(E_F)$ value obtained for $x \leq 4.0$ is 104.5 states.Ry^{-1} per formula unit ($Ba_8Ni_{1.5}Ge_{43}\square_{1.5}$) suggesting that the compositions x = 4.5 and 6.0 may not be stable. Indeed, experimentally, the maximum Ni content is achieved as 4.2 atoms per unit cell.

The observation that the electronic behavior of the clathrate-I $Ba_8Ni_xGe_{46-x-y}\square_y$ is of either $Ba_8Ni_xGe_{43}\square_{3-x}$ or $Ba_8Ni_xGe_{42}\square_{4-x}$ type is further corroborated by an examination of the band structures. Four bands cross the Fermi energy in the case of $Ba_8Ni_xGe_{43}\square_{3-x}$ with x = 0.5, 1.0 and 1.5. The band structure of $Ba_8Ni_{0.5}Ge_{43}\square_{2.5}$, as an example, is presented in Figure 7 (top panel). Here, the two lowest (highest) crossing bands, plotted in blue (red), give rise to holelike (electronlike) Fermi surfaces. The middle panel shows the band structure of $Ba_8Ni_3Ge_{42}\square_1$, as a representative of the x = 2.0, 3.0 and 4.0 cases, where three bands cross the Fermi energy, again with two lowest energy ones (drawn in blue) yielding hole pockets and the third (drawn in red) electron pockets. Finally, Figure 7 (bottom panel) illustrates the band structure of $Ba_8Ni_{4.5}Ge_{41.5}$ as an example for the $x > 4$ case. There are six bands crossing the Fermi energy. The lowest lying two, shown in blue, yield quite large hole pockets around **Γ** and **H**. The highest two, shown in red, form relatively small electron pockets around **P**. The bands shown in green display a more complicated behavior due to degeneracies. On one hand, they form the small electron pockets around **N** and on the other hand, they contribute to the hole pockets.

C. Specific heat

The temperature dependence of the specific heat C_p of $Ba_8Ni_xGe_{46-x-y}\square_y$ is plotted in Figure 8a between 1.9 and 300 K for the illustrative x = 1.0 sample. The Dulong-Petit value $C_p = 3NR$ where N is the number of atoms per formula unit and R is the gas constant is reached at 300 K. The Sommerfeld coefficient, γ, which enables to probe the variations in the density of states at the Fermi level as a function of the Ni content, was inferred from an analysis of the low-temperature data via the conventional free-electron relation $C_p / T = \gamma + \beta T^2$ where βT^2 stands for the phononic contribution. As shown in Figure 8b, the concentration x = 1.0 delineates two distinct evolution of γ with x. Below this value, γ evolves in a non-linear fashion varying between 25 mJ mol^{-1} K^{-2} in the parent compound up to 42 mJ mol^{-1} K^{-2} in the sample with x = 0.9. Above x = 1.0, γ tends to decrease monotonically with increasing Ni content up to x = 4.0 where a minimum value of 4 mJ mol^{-1} K^{-2} is reached before increasing again as the Ni content is slightly enhanced from x = 4.0 to x = 4.1. As discussed in the next paragraphs, the non-linear variation in γ with x is likely related to the sensitivity to the Ni content of the electronlike and holelike band contributions to $N(E_F)$. As the Ni content is increased beyond x = 1.0, the superstructure is no longer visible in PXRD leading to modifications in the electronic band structure. Progressively increasing the Ni content then results in a smooth shift of the Fermi level downwards the conduction bands up to x = 4.0 where a semiconducting state is expected to develop. Note that the γ value does not vanish at this concentration, which may be due to a small off-stoichiometry in the Ni content. Since the x = 4.0 composition is expected to feature a narrow band gap, a small variation around this value may be sufficient to push the Fermi level out of the band gap. Nevertheless, the overall variation in the γ values above x = 1.0 is consistent with an overall decrease of the

DOS at the Fermi level on going from x = 1.0 up to x = 4.0 revealed by band structure calculations. The crossover from an *n*-type to a *p*-type conduction expected to occur for slightly higher Ni contents is also in agreement with the increase in γ observed in the x = 4.1 sample reflecting a shift of the Fermi level towards the valence band edges.

The γ values, listed in Table III, are linked to $N(E_F)$ via the relation $\gamma = 0.173N(E_F)$ with γ and $N(E_F)$ expressed in mJ mol^{-1} K^{-2} and states Ry^{-1}, respectively. The β coefficient is related to the Debye temperature, θ_D, via the relation $\theta_D = \left(\frac{12\pi^4 NR}{5\beta}\right)^{\frac{1}{3}}$. Using the number of atoms derived from WDXS compositions, the θ_D values can be then calculated and are depicted in Figure 8c as a function of the Ni content. As can be observed, θ_D increases upon substituting to fall in the 255 – 275 K temperature range for 0.2 ≤ x ≤ 3.5. Above x = 3.5, the Debye temperatures are significantly higher reaching ~ 300 K. This intriguing change in θ_D might be related to the presence of Ni atoms on both the 6*c* and 24*k* sites of the crystal structure resulting in variations in the bonding scheme at high Ni concentration.

The low-temperature dependence of C_p (5 – 100 K) in type-I clathrates can be usually described on a more quantitative level using a model reflecting Einstein contributions solely associated to the Ba2 atoms over a Debye background.[27-30] This approximation yields the following expression for the lattice contribution to the specific heat C_L

$$C_L = C_D + C_{E_i} = 9Nk_B \int_0^{\frac{\theta_D}{T}} \frac{x^4 e^x}{(e^x - 1)^2} dx + \sum_i p_i N_{E_i} R \left(\frac{\theta_{E_i}}{T}\right)^2 \frac{e^{\theta_{E_i}/T}}{(e^{\theta_{E_i}/T} - 1)^2} \quad (1)$$

where C_D is the contribution associated to the Ni/Ge framework and Ba1 atoms described within the Debye model and C_{E_i} is the Einstein contribution of the i^{th} vibrational mode of the

Ba2 atoms. In Eq.(1), $x = \hbar\omega / k_B T$ with $\hbar$ the reduced Planck constant and k_B the Boltzmann constant, N_D is the number of Debye oscillators per formula unit and p_i, N_{E_i} and θ_{E_i} are the degrees of freedom, the number of Einstein oscillators, and the Einstein temperature related to the i^{th} vibrational mode, respectively. The symmetry of the 6*d* site leads to anisotropic thermal displacement parameters associated to two Einstein temperatures within the present description, $\theta_E^{\parallel}$ and $\theta_E^{\perp}$, which represent the in-plane and out-of-plane thermal motion of the Ba2 atoms, respectively.

This approach was found to be pertinent in most clathrates substituted with transition metals. The resulting Einstein temperatures can be then straightforwardly compared to the low-energy phonon modes revealed *e.g.* by either Raman spectroscopy or inelastic neutron scattering. Though this model has been applied to several $Ba_8M_xGe_{46-x-y}\square_y$ (*M* = Cu, Au, Ag…) compounds for a given *x* content,[31-34] only few studies of the evolution of the Einstein temperatures over a wide range of compositions have been reported so far. This analysis may provide valuable insights into the dynamical motion of the Ba2 atoms as a function of the Ni content *i.e.* as a function of the cage volume. The θ_D along with the $\theta_E^{\parallel}$ and $\theta_E^{\perp}$ values inferred from least-square fits to the data for several Ni-substituted compounds are listed in Table III and the latter are depicted in Figure 8d as a function of *x*. While no clear correlation between $\theta_E^{\perp}$ and *x* can be observed in the present case, the $\theta_E^{\parallel}$ values increase linearly with the Ni content up to *x* = 4.1. No strong variations in these characteristic temperatures occur at the *n*- to *p*-type transition as observed in the $Ba_8Au_xSi_{46-x}$ clathrates.[27] Nevertheless, above *x* = 3.1, the $\theta_E^{\perp}$ values significantly drop from 95 to 75 K following the decrease in the lattice parameter.

D. Electrical resistivity and Hall effect

The temperature dependence of the electrical resistivity is shown in Figure 9. $\rho(T)$ data of the parent compound $Ba_8Ge_{43}\square_3$ is characterized by a maximum centred near 275 K, above which ρ decreases.[16-18] This behavior has been ascribed to temperature-dependent mobilities and concentrations of holes and electrons, both being involved in the electrical conduction in this material.[16] Upon substituting Ge by Ni, this maximum is strongly reduced while still discernable for $x \leq 1.0$. This behavior is also consistent with the idea that holes and electrons still play a role in the electrical conduction below this Ni content. Interestingly, likewise the specific heat data, the dependence of the ρ values on x differs depending on whether the Ni content is lower or higher than $x = 1.0$. Below this content, no clear trend can be observed, ρ first decreasing with x up to $x = 0.6$ before slightly increasing in the $x = 0.9$ and 1.0 samples. As we shall see below, this non-monotonic behavior likely arises due to a shift in the balance between the hole and electron contributions. From $x = 1.0$ to $x = 3.1$, ρ increases as a result of a decrease in the carrier concentration (see below). This trend is confirmed by the data collected on the annealed samples ($x > 3.5$) which shows an increase in ρ as x approaches $x = 4.0$. The metallic-like behavior observed up to $x = 4.0$ then turns into a semiconducting-like one in the $x = 4.1$ sample.

Hall-effect measurements carried out on $Ba_8Ge_{43}\square_3$ between 2 and 350 K have demonstrated that both holes and electrons contribute to the electrical conduction.[16] Specifically, a dominant holelike signal independent of temperature and a significant magnetoresistance were the two prominent signatures of the multiband nature of the electrical conduction classifying $Ba_8Ge_{43}\square_3$ as a nearly-compensated semimetal. In the present system, questions arise as for the variations of these properties with x and their possible link with the partially-ordered vacancies. To address these issues, Hall effect measurements were

performed in the same temperature range paying particular attention to the samples with low Ni content ($x \leq 1.0$).

Up to x = 0.9, the $\rho_{xy}(\mu_0 H)$ data (not shown) retain a positive and linear field dependence in the whole temperature range indicating a dominant holelike response as observed in the parent compound. The multiband conduction featured by $Ba_8Ge_{43}\square_3$ is thus preserved over a significant Ni concentration window in agreement with our first-principles calculations carried out for x = 0.6 and x = 1.0. With a slight increase in the Ni content to x = 1.0, both charge carriers show up and a crossover from a dominant holelike signal to an electronlike contribution occurs between 180 and 250 K. Thus, as observed in the specific heat data, the x = 1.0 concentration represents a border above which an electronlike signal reflected by a negative slope is solely observed. These results further indicate a contribution of electrons to the Hall signal of increasing importance as the Ni content increases.

Figure 10a depicts the temperature dependence of the Hall coefficient R_H inferred from the slope of $\rho_{xy}(\mu_0 H)$ for $x \leq 1.0$. The deep minimum near 275 K characterizing the temperature dependence of R_H in $Ba_8Ge_{43}\square_3$ is strongly weakened upon alloying with Ni but still distinguishable up to x = 0.6. Further, the R_H values decrease with increasing x. Within a single-band picture, R_H is related to the hole and electron concentrations p and n, respectively, via the relations $p = r_H / R_H e$ and $n = -r_H / R_H e$ where r_H is the Hall factor and e is the elementary charge. In principle, r_H depends on the topology of the Fermi surface, on the scattering mechanisms of the charge carriers and on temperature. However, assuming $r_H = 1$ was shown to be a good approximation for clathrates, especially at low temperatures, resulting in the well-known relations $p = 1/R_H e$ and $n = -1/R_H e$. In the present case, these relations give an upper limit of p which increases by one order of magnitude, from 1.4×10^{21} cm^{-3} in the parent compound to 1.0×10^{22} cm^{-3} in the x = 0.8 sample at 200 K.

As mentioned above, the second signature of the multiband conduction in $Ba_8Ge_{43}\square_3$ is related to a significant magnetoresistance $\Delta\rho_{xx}(\mu_0 H,T)/\rho_{xx}(0,T) = [\rho_{xx}(\mu_0 H,T) - \rho_{xx}(0,T)]/\rho_{xx}(0,T)$ where $\rho_{xx}(\mu_0 H,T)$ and $\rho_{xx}(0,T)$ are the longitudinal resistivity at a magnetic field $\mu_0 H$ and that at zero magnetic field, respectively. The evolution of the temperature dependence of the magnetoresistance with the Ni content is depicted in Figure 10b. With increasing *x*, its magnitude decreases below 1% except for the *x* = 0.6 sample where a rise in the values towards low temperatures is observed. The *x* = 0.2, *x* = 0.9 and *x* = 1.0 samples share a similar temperature dependence characterized by a minimum near 200 K, a feature also present in the parent compound. The variation in temperature of $\Delta\rho_{xx}/\rho_{xx}$ of the *x* = 0.6 sample is somewhat stronger, the values being negligibly small between 300 and 200 K and increasing with decreasing temperature to reach 1.7% at 10 K.

The presence of both holes and electrons naturally raises the question to which extent a description within a two-band model is relevant in the present case. In $Ba_8Ge_{43}\square_3$, this model yielded large mobilities along with nearly equivalent concentrations of electrons and holes, consistent with the nearly-compensated behavior of the thermopower.[16] However, this model was found to overestimate the mobilities of both carriers at low temperatures. Applying the model used to analyze the galvanomagnetic data of $Ba_8Ge_{43}\square_3$, an estimation of the hole and electron concentrations and mobilities together with their temperature dependences for different Ni contents up to *x* = 1.0 could be obtained. In the present case, this model could not be applied to the *x* = 0.6 sample above 200 K and to the *x* = 0.9 sample due to the very small magnetoresistive signal recorded. The results (not shown) evidence an increase in both the electron and hole concentrations as well as a strong decrease of the mobilities with increasing the Ni content.

Above *x* = 1.0, further increasing Ni content no longer influences the sign of the

$\rho_{xy}(\mu_0 H)$ data which remains negative up to x = 4.0 (not shown) indicating that electrons become the main charge carriers. The second transition from *n*-type to *p*-type conduction is then driven by a slight increase in x from x = 4.0 to x = 4.1 as demonstrated by the positive slope of the Hall data in the latter sample. Figure 11a shows n as a function of the Ni content for $x > 1.0$ derived from the above-mentioned single-band relation. As can be seen, n decreases with increasing x as expected in a progressive metal-insulator transition. These results are consistent with previous investigations and with our specific heat data indicating a decrease in $N(E_F)$ with x.

The temperature dependence of the Hall mobility of the electrons, defined as $\mu_H = R_H / \rho$, is depicted in Figure 11b for the samples with x = 2.1, 3.1, 3.5 and 4.0. μ_H is practically temperature-independent regardless of the composition. This indicates that neutral-impurity scattering ($\mu_H \propto cst$) is the main scattering mechanism limiting the carrier mean-free path in the present system. Some compositions show a slight decrease near room temperature probably reflecting the effect of acoustic-phonon scattering ($\mu_H \propto T^{-3/2}$), which usually dominates at higher temperatures. Our $\mu_H(T)$ data are in agreement with Hall-effect measurements carried out on $Ba_8Ni_yGa_zGe_{46-y-z}$ for which a progressive evolution from acoustic-phonon scattering in the Ni-free compound (z = 16) towards neutral-impurity scattering in the Ga-free compound (y = 4) has been observed.[10]

E. Thermopower and thermal conductivity

Figures 12a and 12b show the temperature dependence of the thermopower for all the samples investigated. At low Ni concentrations ($x < 0.9$), the temperature dependence of α resembles that of the parent $Ba_8Ge_{43}\square_3$ compound characterized by two transitions from *n*-

type to *p*-type conduction. This complex temperature dependence, which originates from the simultaneous presence of holes and electrons smoothly evolves upon alloying with Ni towards pure *n*-type conduction. For x = 0.2 and x = 0.6, the low-temperature maximum in $|\alpha|$ disappears while the maximum centred around 225 K in $Ba_8Ge_{43}\square_3$ still exists.[16-18] This maximum is slightly shifted towards lower temperatures up to x = 0.6 and is no longer visible at x = 0.9. A transition from *p*-type to *n*-type behavior then occurs near room temperature in both x = 0.2 and x = 0.6 compounds. For x = 0.9 and x = 1.0, the thermopower values remain negative in the whole temperature range and are close to zero below 150 K suggesting a nearly perfect compensation of the hole and electron contributions to α. The increase in the magnitude of α with increasing x above x = 1.0 reflects the decrease in the electron concentration and is consistent with a progressive metal-semiconductor transition. At high Ni concentration (x > 3.1), $|\alpha|$ increases quasi-linearly with temperature indicative of a diffusive nature. A slight increase in the Ni concentration from x = 4.0 to x = 4.1 drives the system to a *p*-type conduction characterized by positive thermopower values. The non-linear dependence observed for x = 4.1 further indicates a non-degenerate behavior in agreement with $\rho(T)$ data. The upturn observed above ~ 300 K likely indicates the onset of the thermal activation of minority carrier which leads to a decrease of the magnitude of α with increasing temperature. From the maximum thermopower value α_{max} and the temperature at which this maximum occurs T_{max}, the thermal band gap E_g can be estimated using $E_g = 2e\alpha_{max}T_{max}$ yielding a band gap of ~ 65 meV. The overall variation in the transport properties of $Ba_8Ni_xGe_{46-x-y}\square_y$ samples show trends typical of heavily doped semiconductors evolving towards non-degenerate semiconductors as x increases. As demonstrated in Ref. 14, the samples remain degenerate up to x = 3.5 *i.e.* for n higher than approximately 1.6×10^{21} cm^{-3}. At higher Ni contents, the degenerate statistics can no longer be applied and the loss of

degeneracy must be taken into account when deriving the basic features of transport such as the effective masses and the Lorenz number.

The temperature dependence of the total thermal conductivity is reported in Figures 13a and 13b. The temperature dependence of the binary compound features a pronounced low-temperature dielectric maximum followed by a strong decrease with T typical of crystalline materials. A small addition of Ni results in a strong drop in the κ values that then only slightly vary upon further alloying. The amplitude of the crystalline peak observed at low temperatures is strongly lowered upon filling up of the vacancies with Ni. The vacancies in the Ge framework are surrounded by Ge^- anions, which can be expected to show a distinct interaction with the Ba atoms. A more homogeneous charge distribution in the framework might thus induce structural disorder concerning the Ba position in the cages. Above x = 1.0, the thermal conductivity further decreases even though the superstructure disappears. This behavior is a direct consequence of the increase in the electrical resistivity values thereby decreasing the electronic contribution κ_e to the thermal conductivity. The values measured in samples containing high Ni levels ($x \geq 2.1$) thus almost entirely reflect the lattice contribution κ_l. This is further corroborated by the temperature dependence of κ_l obtained after subtracting the electronic contribution using the Wiedemann-Franz law $\kappa_e = LT/\rho$ where L is the Lorenz number. A more accurate assessment of κ_l can be obtained by explicitly taking into account the loss of degeneracy when the Fermi level nears the conduction band edge *i.e.* when the Ni content approaches x = 4.0. Herein, the Lorenz numbers calculated (supposed to be temperature-independent below 300 K) within a single-parabolic-band model in Ref. 14 have been utilized to estimate κ_l.

As shown in Figures 14a and 14b, the κ_l values of the Ni-substituted compounds are significantly lower than that of $Ba_8Ge_{43}\square_3$. κ_l remains practically unchanged when the Ni

content spans the range $0.2 \leq x \leq 3.1$ and is in line with values usually encountered in other Ge-based type-I clathrates (Table III).[2] Above $x = 3.5$, the samples show a more pronounced crystalline peak with respect to the $x = 2.1$ and 3.1 samples. This may be attributed to the annealing treatment, which increases the crystallinity and modifies the microstructure (*i.e.* grain size) compared to the splat-cooled samples. More intriguing is the fact that a slight increase in the Ni content from $x = 4.0$ to $x = 4.1$ is then sufficient to suppress the low-temperature maximum leading to a temperature dependence which resembles that of glassy systems. This result is in agreement with the data of Johnsen *et al.*[11] collected on samples with nominal compositions $Ba_8Ni_{6-x}Ge_{40+x}$ ($0 \leq x \leq 0.6$) where a crossover from a crystalline to a glass-like dependence was observed. These results indicate that this dependence is an intrinsic property of the *p*-type sample.

This crossover is not confined to the $Ba_8Ni_xGe_{46-x-y}\square_y$ phase and has been already observed in other type-I clathrates such as in *n*-type and *p*-type $Ba_8Ga_{16}Ge_{30}$, *n*-type $Sr_8Ga_{16}Ge_{30}$, *n*-type $Eu_8Ga_{16}Ge_{30}$, *p*-type $Ba_8Ga_{16}Sn_{30}$ and in *p*-type $Ba_8Au_xSi_{46-x}$ samples.[27, 35-40] Several mechanisms have been discussed in the literature to explain such a difference in the thermal transport between *n*-type and *p*-type samples. The mechanisms invoked are either associated to the off-center position of the guest atoms (Ba, Eu or Sr) in the tetrakaidecahedra or to a strong phonon-charge carrier coupling. The former property leads to the presence of tunnelling states which dominate at low temperatures and can be unveiled by a T^2 dependence of the thermal conductivity at very low temperatures (typically $T < 1$ K) or by specific heat data which features an additional contribution superimposed to the electronic one.[40,41] In the present case, the variation in the experimental γ values with *x* is well reproduced by first-principles calculations suggesting the absence of tunnelling states in the present system. The second mechanism, which may be at play in the present case, has been suggested by Johnsen *et al.*[11] to explain the different behavior observed between *n*- and *p*-type $Ba_8Ni_{6-x}Ge_{40+x}$. The

larger m^* value in the x = 4.1 sample (estimated to $9\,m_0$, see Ref. 14) seems consistent with the idea of an enhanced phonon scattering on charge carriers with respect to the *n*-type samples. In the $Ba_8Au_xSi_{46-x}$ system,[27] it has been suggested that, besides a possible enhanced hole-phonon coupling, a higher degree of disorder in the crystal lattice may also play an important role. This disorder originates from a mixed occupation of both the 6*c* and 24*k* sites of the crystal structure by Au and Si atoms as shown by single-crystal x-ray diffraction analyses.[42] Whether a similar mixed occupation occurs for Ni and Ge remains to be experimentally confirmed. Another possibility could be that the presence of anions would result in a lock-in position of the Ba atoms. The complete disappearance of these anions in *p*-type samples would then release the Ba atoms thereby leading to stronger coupling between the Ba phonon modes and those of the cages, in agreement with recent inelastic neutron scattering experiments.[43] Finally, it is noteworthy that a similar disappearance of the crystalline peak occurs in skutterudite compounds upon filling the cages with different elements even though the thermal conductivity retains a conventional behavior.[44] Hence, to classify the present *p*-type clathrate as a real example of glass-like behavior may be premature and would require thermal conductivity measurements at lower temperatures.

IV. Conclusion

We have reported a joint experimental and theoretical investigation of the evolution of the transport properties in the $Ba_8Ni_xGe_{46-x-y}\square_y$ type-I clathrate system. The structural and chemical characterizations revealed a significantly different homogeneity range from previously reported extending from x = 0.0 to x = 4.2. Measurements of the specific heat, electrical resistivity, Hall effect, thermopower and thermal conductivity were carried out for different Ni concentrations spanning the whole homogeneity range. Analysis of the Hall-

effect data indicates a smooth evolution of the nearly-compensated semi-metallic state of $Ba_8Ge_{43}\square_3$ below this content towards a conventional, single-carrier metallic state above. As the Ni concentration approaches x = 4.0, the system is driven towards a metal-insulator transition in agreement with our first-principles calculations. A crossover from *n*-type to *p*-type electrical conduction is achieved at slightly higher Ni content *i.e.* for x = 4.1. Our theoretical study has suggested significant differences in the electronic band structure between *n*-type and *p*-type compounds reflected by flatter bands near the Fermi level in the latter. This strong change is consistent with larger effective masses of the charge carrier in the *p*-type sample.[14] The $Ba_8Ni_xGe_{46-x-y}\square_y$ system represents another example of clathrates where tuning the electrical conduction is accompanied by a profound change in the thermal transport. The synthesis route used in the present study opens up the possibility to access low substitution levels and may be extended to other transition metals allowing a systematic study of the nearly-compensated semi-metallic state of $Ba_8Ge_{43}\square_3$ upon filling up of the vacancies.

Acknowledgment

The authors would like to thank the members of the Kompetenzgruppe Struktur at MPI-CPfS for providing experimental support. C.C. acknowledges the financial support of the CNRS-MPG program. A.O. would like to thank Ulrike Nitzsche at Leibnitz Institute IFW Dresden for technical support regarding electronic structure calculations. Yu.G. gratefully acknowledges financial support by the Deutsche Forschungsgemeinschaft (SPP 1386).

References

[1] M. Falmbigl and P. Rogl in Thermoelectrics and its Energy Harvesting, edited by D. M. Rowe (CRC Press, 2012).

[2] M. Christensen, S. Johnsen and B. B. Iversen, *Dalton Trans.* 2010, **39**, 978.

[3] K. A. Kovnir and A. V. Shevelkov, *Russ. Chem. Rev.* 2004, **73**, 923.

[4] G. S. Nolas, G. A. Slack and S. B. Schujman in *Semiconductors and Semimetals*, ed. T.M. Tritt vol. 69, 255 (2001).

[5] J. L. Cohn, G. S. Nolas, V. Fessatidis, T. H. Metcalf and G. A. Slack, *Phys. Rev. Lett.* 1999, **82**, 779.

[6] H.J. Goldsmid in *Thermoelectric Refrigeration* (Temple Press Books Ltd, London, 1964).

[7] G. Miller in *Chemistry, Structure and Bonding of Zintl Phases and Ions* (VCH Publishers Inc.: New-York, 1996), S. M. Kauzlarich Ed.

[8] E. S. Toberer, M. Christensen, B. B. Iversen and G. J. Snyder, *Phys. Rev. B* 2008, **77**, 075203.

[9] H. Zhang, H. Borrmann, N. Oeschler, C. Candolfi, W. Schnelle, M. Schmidt, U. Burkhardt, M. Baitinger, J.-T. Zhao and Yu. Grin, *Inorg. Chem.* 2011, **50**, 1250.

[10] X. Shi, J. Yang, S. Bai, J. Yang, H. Wang, M. Chi, J. R. Salvador, W. Zhang, L. Chen and W. Wong-Ng, *Adv. Funct. Mater.* 2010, **20**, 755.

[11] S. Johnsen, A. Bentien, G. K. H. Madsen, M. Nygren and B. B. Iversen, *Phys. Rev. B* 2007, **76**, 245126.

[12] A. Bentien, S. Johnsen and B. B. Iversen, *Phys. Rev. B* 2006, **73**, 094301.

[13] J. Xu, J. Wu, S. Heguri, G. Mu, Y. Tanabe and K. Tanigaki, *J. Electron. Mater.* 2012, **41**, 1177; J. Xu, J. Wu, Y. Tanabe, S. Heguri, G. Mu, H. Shimatori, K. Tanigaki, *J. Electron.*

Mater. 2013, **42**, 2025.

[14] U. Aydemir, C. Candolfi, A. Ormeci, M. Baitinger, N. Oeschler, F. Steglich and Yu. Grin, *J. Phys.: Condens. Matter* 2014, **26**, 485801.

[15] L. T. K. Nguyen, U. Aydemir, M. Baitinger, E. Bauer, H. Borrmann, U. Burkhardt, J. Custers, A. Haghighirad, R. Höfler, K. D. Luther, F. Ritter, W. Assmus, Yu. Grin and S. Paschen, *Dalton Trans.* 2010, **39**, 1071.

[16] C. Candolfi, A. Ormeci, U. Aydemir, M. Baitinger, N. Oeschler, Yu. Grin and F. Steglich, *Phys. Rev. B* 2011, **84**, 205118.

[17] C. Candolfi, U. Aydemir, M. Baitinger, N. Oeschler, F. Steglich and Yu. Grin, *J. Electron. Mater.* 2010, **39**, 2039.

[18] U. Aydemir, C. Candolfi, H. Borrmann, M. Baitinger, A. Ormeci, W. Carrillo-Cabrera, C. Chubilleau, B. Lenoir, A. Dauscher, N. Oeschler, F. Steglich and Yu. Grin, *Dalton Trans.* 2010, **39**, 1078.

[19] U. Aydemir, C. Candolfi, A. Ormeci, H. Borrmann, U. Burkhardt, Y. Oztan, N. Oeschler, M. Baitinger, F. Steglich and Yu. Grin, *Inorg. Chem.* 2012, **51**, 4730.

[20] K. Koepernik and H. Eschrig, *Phys. Rev. B* 1999, **59**, 1743.

[21] P. Perdew and Y. Wang, *Phys. Rev. B* 1992, **45**, 13244.

[22] H. Zhang, J.-T Zhao, M.-B. Tang, Z.-Y. Man, H.-H. Chen and X.-X. Yang, *J. Phys. Chem. Solids* 2009, **70**, 312.

[23] G. Cordier and P. Woll, *J. Less-Comm. Met.* 1991, **169**, 291.

[24] A. N. Mansour and C. A. Melendres, *J. Phys. Chem. A* 1998, **102**, 65.

[25] M. Crespin, P. Levitz, L. Gatineau, *J. Chem. Soc., Faraday Trans. 2* 1983, **79**, 1181.

[26] J. Zhao, A. Buldum and J. P. Lu, *Phys. Rev. B* 1999, **60**, 14177.

[27] U. Aydemir, C. Candolfi, A. Ormeci, Y. Oztan, M. Baitinger, N. Oeschler, F. Steglich and Yu. Grin, *Phys. Rev. B* 2011, **84**, 195137.

[28] K. Suekuni, M. A. Avila, K. Umeo, and T. Takabatake, *Phys. Rev. B* 2007, **75**, 195210.

[29] A. Bentien, E. Nishikori, S. Paschen and B. B. Iversen, *Phys. Rev. B* 2005, **71**, 144107.

[30] S. Paschen, W. Carrillo-Cabrera, A. Bentien, V. H. Tran, M. Baenitz, Y. Grin, and F. Steglich, *Phys. Rev. B* 2001, **64,** 214404.

[31] M. Christensen and B. B. Iversen, *J. Phys.: Condens. Matter* 2008, **20**, 104244.

[32] N. Melnychenko-Koblyuk, A. Grytsiv, P. Rogl, M. Rotter, E. Bauer, G. Durand, H. Kaldarar, R. Lackner, H. Michor, E. Royanian, M. M. Koza and G. Giester, *Phys. Rev. B* 2007, **76**, 144118.

[33] N. Melnychenko-Koblyuk, A. Grytsiv, P. Rogl, M. Rotter, R. Lackner, E. Bauer, L. fornasari, F. Marabelli and G. Giester, *Phys. Rev. B* 2007, **76**, 195124.

[34] S. Johnsen, M. Christensen, B. Thomsen, G. K. H. Madsen and B. B. Iversen, *Phys. Rev. B* 2010, **82**, 184303.

[35] A. Bentien, M. Christensen, J. D. Bryan, A. Sanchez, S. Paschen, F. Steglich, G. D. Stucky, and B. B. Iversen, *Phys. Rev. B* 2004, **69,** 045107.

[36] M. Christensen, N. Lock, J. Overgaard, and B. B. Iversen, *J. Am. Chem. Soc.* 2006, **128,** 15657.

[37] M. A. Avila, K. Suekuni, K. Umeo, H. Fukuoka, S. Yamanaka, and T. Takabatake, *Phys. Rev. B* 2006, **74,** 125109.

[38] B. C. Sales, B. C. Chakoumakos, R. Jin, J. R. Thompson, and D. Mandrus, *Phys. Rev. B* 2001, **63,** 245113.

[39] K. Suekuni, M. A. Avila, K. Umeo, H. Fukuoka, S. Yamanaka, T. Nakagawa, and T. Takabatake, *Phys. Rev. B* 2008, **77** 235119.

[40] M. A. Avila, K. Suekuni, K. Umeo, H. Fukuoka, S. Yamanaka, and T. Takabatake, *Appl. Phys. Lett.* 2008, **92,** 041901.

[41] J. Xu, J. Tang, K. Sato, Y. Tanabe, H. Miyasaka, M. Yamashita, S. Heguri, and K. Tanigaki, *Phys. Rev. B* 2010, **82,** 085206.

[42] N. Jaussaud, P. Gravereau, S. Pechev, B. Chevalier, M. Ménétrier, P. Dordor, R. Decourt, G. Goglio, C. Cros, and M. Pouchard, *C. R. Chimie* 2005, **8**, 39.

[43] H. Euchner, S. Pailhès, L. T. K. Nguyen, W. Assmus, F. Ritter, A. Haghighirad, Yu. Grin, S. Paschen, M. de Boissieu, *Phys. Rev. B* 2012, **86**, 224303.

[44] C. Uher, in *Semiconductors and Semimetals*, edited by T. Tritt (Academic, San Diego, 2000), Vol. 69, p. 139 and in *Thermoelectrics and its Energy Harvesting*, edited by D. M. Rowe (CRC, 2012), Chap. 10.

Tables

Table I. Compositions of the $Ba_8Ni_xGe_{46-x-y}\square_y$ models considered and space groups used in the first-principles calculations. The lattice parameters and density of states at Fermi energy are also provided. The preferred compositions according to balances (1) and (2) are indicated by the symbol + and the lowest energy cases by the symbol *.

Composition	*Space group*	*Lattice parameters (Å)*	*$N(E_F)$ (States $Ry^{-1}(fu)^{-1}$)*
$Ba_8Ni_{0.5}Ge_{42.5}\square_3$	$I\bar{4}c2$ (no. 120)	$a = b = c = 21.3083$	104.8
$Ba_8Ni_{0.5}Ge_{43}\square_{2.5}$	$I\bar{4}c2$ (no. 120)	$a = b = c = 21.3083$	49.7 (+)
$Ba_8Ni_{1.0}Ge_{42}\square_3$	$I4_1/acd$ (no. 142)	$a = b = c = 21.3083$	61.9
$Ba_8Ni_{1.0}Ge_{43}\square_2$	$I4_1/acd$ (no. 142)	$a = b = c = 21.3083$	53.3 (+)
$Ba_8Ni_{1.5}Ge_{41.5}\square_3$	$I\bar{4}3d$ (no. 220) $I\bar{4}_132$ (no. 214)	$a = 21.3083$ $a = 21.3083$	293.3 (*) 293.6
$Ba_8Ni_{1.5}Ge_{42}\square_{2.5}$	$I\bar{4}c2$ (no. 120)	$a = b = c = 21.3083$	64.5
$Ba_8Ni_{1.5}Ge_{43}\square_{1.5}$	$I\bar{4}3d$ (no. 220) $I\bar{4}_132$ (no. 214)	$a = 21.3083$ $a = 21.3083$	778.8 104.5 (+)
$Ba_8Ni_{2.0}Ge_{42}\square_2$	$I4_1/acd$ (no. 142) $P4_122$ (no. 90)	$a = b = c = 21.3364$ $a = b = 10.6682$; $c = 2a$	93.2 (+) 109.0
$Ba_8Ni_{2.0}Ge_{43}\square_1$	$I4_1/acd$ (no. 142)	$a = b = c = 21.3364$	171.4
$Ba_8Ni_{3.0}Ge_{42}\square_1$	$I4_1/acd$ (no. 142)	$a = b = c = 21.3538$	48.4 (+)
$Ba_8Ni_{3.0}Ge_{43}$	$Ia\bar{3}d$ (no. 230)	$a = 21.3538$	156.0
$Ba_8Ni_{4.0}Ge_{42}$	$P4_122$ (no. 91)	$a = b = 10.6784$; $c = 2a$	58.1
$Ba_8Ni_{4.5}Ge_{41.5}$	$I\bar{4}3d$ (no. 220) $I\bar{4}_132$ (no. 214)	$a = 21.3568$ $a = 21.3568$	308.9 (*) 220.6

$Ba_8Ni_6Ge_{40}$ a)	$Pm\bar{3}n$ (no. 223)	a = 10.5097		316.6

a) The atomic and the lattice parameters for this model were fully optimized.

Table II. Actual compositions, nature of the secondary phases (< 3 wt.%) and lattice parameters (a) of the $Ba_8Ni_xGe_{46-x-y}\square_y$ compounds. For each sample, the amount of by-products estimated from PXRD is also given. For comparison purposes, data from prior studies have been added.

Nominal composition	*WDXS*	*Secondary phases*	*a (Å)*	*Reference*
Ba_8Ge_{43}	$Ba_{8.00(1)}Ge_{42.99(4)}$	C-I (100 %)	21.3079(2) (a/2 = 10.6540)	
$Ba_8Ni_{0.2}Ge_{42.8}$	$Ba_{8.00(2)}Ni_{0.19(2)}Ge_{42.89(3)}$	C-I (> 97%) + α-Ge (< 3%)	21.3085(3) (a/2 = 10.6543)	
$Ba_8Ni_{0.5}Ge_{42.5}$	$Ba_{8.0(1)}Ni_{0.6(2)}Ge_{42.7(2)}$	C-I (> 99%) + α-Ge (<1%)	21.3140(2) (a/2 = 10.6570)	
$Ba_8Ni_{0.5}Ge_{43}$	$Ba_{8.00(2)}Ni_{0.6(1)}Ge_{43.1(1)}$	C-I (>99%) + α-Ge (<1%)	21.3108(2) (a/2 = 10.6554)	
$Ba_8Ni_{0.8}Ge_{42.2}$	$Ba_{8.0(1)}Ni_{0.9(2)}Ge_{42.5(2)}$	C-I (>99%) + α-Ge (<1%)	21.1.93151(2) (a/2 = 10.6576)	
$Ba_8Ni_{1.0}Ge_{42.0}$	$Ba_{8.0(1)}Ni_{1.0(2)}Ge_{43.1(3)}$	C-I (>97%) + Ba_6Ge_{25} (<3%)	21.3166(2) (a/2 = 10.6583)	
$Ba_8Ni_{1.0}Ge_{43.0}$	$Ba_{8.0(1)}Ni_{1.0(2)}Ge_{42.7(2)}$	C-I + α-Ge	21.3189(2) (a/2 = 10.6595)	
$Ba_8Ni_{1.2}Ge_{43.0}$	$Ba_{8.0(1)}Ni_{1.5(2)}Ge_{42.8(3)}$	C-I + α-Ge	10.6601(4)	
$Ba_8Ni_{2.0}Ge_{42.0}$	$Ba_{8.0(1)}Ni_{2.1(2)}Ge_{43.0(3)}$	C-I (>99%) + Ba_6Ge_{25} (<1%)	10.6678(1)	
$Ba_8Ni_{3.0}Ge_{42.0}$	$Ba_{8.00(3)}Ni_{3.07(2)}Ge_{42.45(3)}$	C-I (100%)	10.6788(1)	
$Ba_8Ni_{3.5}Ge_{42.0}$	$Ba_{8.00(2)}Ni_{3.49(5)}Ge_{42.34(5)}$	C-I (100%)	10.6803(1)	
$Ba_8Ni_{3.8}Ge_{42.0}$	$Ba_{8.00(3)}Ni_{3.90(1)}Ge_{42.03(4)}$	C-I (>97%) + α-Ge (<3%)	10.6787(1)	
$Ba_8Ni_{4.0}Ge_{42.0}$	$Ba_{8.0(1)}Ni_{4.0(2)}Ge_{42.0(1)}$	C-I (>99%) + α-Ge (<1%)	10.6780(1)	
$Ba_8Ni_{4.2}Ge_{41.8}$	$Ba_{8.00(3)}Ni_{4.08(1)}Ge_{41.87(3)}$	C-I (>99%) + α-Ge (<1%)	10.6771(1)	
$Ba_8Ni_6Ge_{40}$	$Ba_{8.00(2)}Ni_{4.22(1)}Ge_{41.29(7)}$	C-I (>90%) + α-Ge (<6%) + $BaGe_2$ (<4%)	10.6765(1)	

$Ba_8Ni_4Ge_{42}$	$Ba_{8.00(3)}Ni_{3.45(2)}Ge_{42.31(4)}$	C-I		10.6798(2)	[15]
$Ba_8Ni_6Ge_{40}$				10.6764(3)	
$Ba_8Ni_{5.8}Ge_{40.2}$	-		-	10.6776(3)	[11]
$Ba_8Ni_{5.6}Ge_{40.4}$				10.6795(2)	
$Ba_8Ni_{5.4}Ge_{40.6}$				10.6807(4)	
$Ba_8Ni_6Ge_{40}$	-		-	10.676(5)	[23]
$Ba_8Ni_6Ge_{40}$	-		-	10.5179(4)	[22]
$Ba_8Ni_3Ge_{43}$				10.6794(5)	
$Ba_8Ni_4Ge_{42}$	-		-	10.6793(5)	[13]
$Ba_8Ni_6Ge_{40}$				10.6752(5)	
$Ba_8Ni_5Ge_{40}$	-		-	10.6780(1)	[13]

Table III. Values of the γ and β parameters inferred from low temperature specific heat analyses. The experimental and theoretical total DOS values $N(E_F)_{Exp}$ and $N(E_F)_{FPLO}$ together with the Debye temperatures θ_D derived from the β parameters are also given. For comparison purposes, the values of the binary $Ba_8Ge_{43}\square_3$ compound (x = 0.0, from Ref. 18 for the experimental value and from Ref. 16 for the theoretical value) have been added.

Actual Ni content	γ (mJ.mol^{-1}.K^{-2})	β (mJ.mol^{-1}.K^{-4})	$N(E_F)_{\exp}$ (states.Ry^{-1}f.u.$^{-1}$)	$N(E_F)_{FPLO}$ (states.Ry^{-1}f.u.$^{-1}$)	θ_D (K)
0.0	24.6	7.93	142.2	35.4	232
0.2	33.2	6.20	191.9	/	252
0.6	27.6	6.05	159.5	49.7	254
0.9	41.3	5.15	238.7	/	268
1.0	32.6	5.33	188.4	53.3	265
2.1	26.3	4.91	152.0	93.2	274
3.1	24.2	5.79	139.9	48.4	261
3.5	20.0	5.00	115.6	/	275
3.9	14.6	3.66	84.4	/	306
4.0	4.5	3.89	26.0	58.1	300
4.1	4.8	3.70	27.7	/	305

Figure Captions

Figure 1: Crystal structure of the type-I $Ba_8Ni_xGe_{46-x-y}\square$ clathrates. The unit cell is composed of a four-bonded Ge/Ni framework with voids forming two pentagonal dodecahedra (in blue) and six tetrakaidecahedra (in green). The framework atoms are located at the Wyckoff sites 6*c* (¼, 0, ½) (white), 16*i* (*x*, *x*, *x*) (grey) and 24*k* (0, *y*, *z*) (orange) while the guest atoms are located at the 2*a* (0, 0, 0) (black) and 6*d* (¼, ½, 0) (purple) sites.

Figure 2: Variations in the lattice parameter *a* (unit cell of the basic clathrate-I structure) of the clathrate $Ba_8Ni_xGe_{46-x-y}\square_y$ as a function of *x* in the nominal compositions: (□) C-I with superstructure, (■) basic C-I structure, (⬟) Ref 13, (▼) Ref 15, (◀) Ref. 11, (▶) Ref. 23. For most of these samples, the standard deviations of the lattice parameters are smaller than the size of the symbols used. The highest limit of the Ni content was determined from WDXS analyses to be 1.0 Ni atom per formula unit for the C-I superstructure and 4.2 Ni atoms per formula unit for the basic C-I structure.

Figure 3: Normalized Ni *K*-edge XANES spectra: (a) clathrates with nominal compositions $Ba_8Ni_1Ge_{42}$, $Ba_8Ni_2Ge_{42}$, $Ba_8Ni_3Ge_{42}$, $Ba_8Ni_{3.5}Ge_{42}$, $Ba_8Ni_4Ge_{42}$, and $Ba_8Ni_6Ge_{40}$. (b) Comparison of the spectra measured for $Ba_8Ni_4Ge_{42}$, Ni foil, NiGe, NiO and NiI_2.

Figure 4: Energy dependence of the total electronic DOS near the Fermi level of the clathrate $Ba_8Ni_xGe_{43}\square_{3-x}$ with x = 0.0, 0.5, 1.0 and 1.5. The vertical dashed line at 0 eV stands for the Fermi level.

Figure 5: Energy dependence of the total electronic DOS near the Fermi level of the clathrate $Ba_8Ni_xGe_{42}\square_{4-x}$ with x = 1, 2, 3 and 4. The vertical dashed line at 0 eV stands for the Fermi level.

Figure 6: Energy dependence of the total electronic DOS near the Fermi level of the clathrates $Ba_8Ni_xGe_{43}\square_{3-x}$ (x = 1.5), $Ba_8Ni_4Ge_{42}$, $Ba_8Ni_{4.5}Ge_{41.5}$ and $Ba_8Ni_6Ge_{40}$. The vertical dashed line at 0 eV stands for the Fermi level.

Figure 7: Electron energy dispersion curves along high symmetry directions near the Fermi level of the clathrates $Ba_8Ni_{0.5}Ge_{43}\square_{2.5}$ (top), $Ba_8Ni_3Ge_{42}\square_1$ (middle) and $Ba_8Ni_{4.5}Ge_{41.5}$ (bottom).

Figure 8: (a) Temperature dependence of the specific heat C_p of $Ba_{8.0(1)}Ni_{1.0(2)}Ge_{43.1(3)}$. The solid black line stands for the theoretical value following the Dulong-Petit law. (b) Sommerfeld coefficient, γ, as a function of the Ni content in $Ba_8Ni_xGe_{46-x-y}\square_y$. The ■ symbol refers to the zero value expected in the semiconducting state for x = 4.0. (c) Debye temperatures θ_D and (d) Einstein temperatures $\theta_E^{\parallel}$ (●) and $\theta_E^{\perp}$ (■) as a function of the Ni content in $Ba_8Ni_xGe_{46-x-y}\square_y$.

Figure 9: Temperature dependence of the electrical resistivity of $Ba_8Ni_xGe_{46-x-y}\square_y$: (a) x = 0 (○), x = 0.2 (□), x = 0.6 (◊), x = 0.9 (Δ), x = 1.0 (●), x = 2.1 (+) and x = 3.1 (▼) and (b) x = 3.5 (♦), x = 3.9 (■), x = 4.0 (▲) and x = 4.1 (▼).

Figure 10: (a) Hall coefficient R_H as a function of T for $x = 0$ (○), $x = 0.2$ (□), $x = 0.6$ (◊), $x = 0.9$ (Δ) and $x = 1.0$ (●). (b) Temperature dependence of the magnetoresistance measured at $\mu_0 H = 7$ T. The symbols used are the same as in panel (a).

Figure 11: (a) Electron concentration n as a function of the Ni content in $Ba_8Ni_xGe_{46-x-y}\square_y$. The symbol ■ refers to the hole concentration p measured in the $x = 4.1$ sample while the ▲ symbol corresponds to the value obtained in a single crystal (Ref. 15). (b) Temperature dependence of the Hall mobility μ_H of $Ba_8Ni_xGe_{46-x-y}\square_y$ for $x = 2.1$ (+), $x = 3.1$ (▼), $x = 3.5$ (♦) and $x = 4.0$ (▲).

Figure 12: Temperature dependence of the thermopower of $Ba_8Ni_xGe_{46-x-y}\square_y$ for (a) $x = 0$ (○), $x = 0.2$ (□), $x = 0.6$ (◊), $x = 0.9$ (Δ), $x = 1.0$ (●), $x = 2.1$ (+) and $x = 3.1$ (▼) and (b) for $x = 3.5$ (♦), $x = 3.9$ (■), $x = 4.0$ (▲) and $x = 4.1$ (▼).

Figure 13: Temperature dependence of the thermal conductivity of $Ba_8Ni_xGe_{46-x-y}\square_y$ for (a) $x = 0$ (○), $x = 0.2$ (□), $x = 0.6$ (◊), $x = 0.9$ (Δ), $x = 1.0$ (●), $x = 2.1$ (+) and $x = 3.1$ (▼) and (b) for $x = 3.5$ (♦), $x = 3.9$ (■), $x = 4.0$ (▲) and $x = 4.1$ (▼).

Figure 14: Temperature dependence of the electronic (a) and lattice (b) thermal conductivity of $Ba_8Ni_xGe_{46-x-y}\square_y$ for $x = 0$ (○), $x = 0.2$ (□), $x = 0.6$ (◊), $x = 0.9$ (Δ), $x = 1.0$ (●), $x = 2.1$ (+), $x = 3.1$ (▼), $x = 3.5$ (♦), $x = 3.9$ (■), $x = 4.0$ (▲) and $x = 4.1$ (▼).

Graphical Abstract

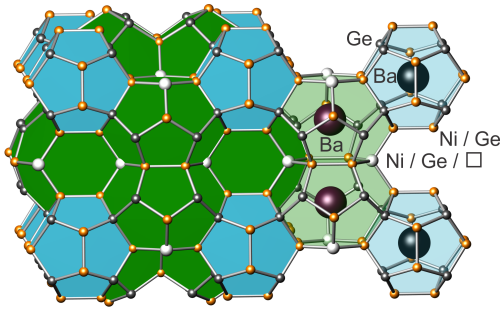

This work reports a comprehensive study of the low-temperature transport properties of the type-I clathrates $Ba_8Ni_xGe_{46-x-y}\square_y$ in the homogeneity range ($0 \leq x \leq 4.1$).